Journal or Quantitative Slrctroscopy & Radiative Transfer 287 (2022) 108223

Contents lists available at ScienceDirect

Journal of Quantitative Spectroscopy & Radiative Transfer

journal homepage: www.elsevier.com/locate/jqsrt

Measurements of elastic light-scattering patterns and images of single, oriented, optically trapped particles

Jessica A. Arnold Aimable Kalume [a], Hairou Yu [b], Christopher L. Wirth [b], Gorden Videena,c,d,e Yong-Le Pan [a]

DEVCOM Anny Research 2800 Mill Road, AddPhi, MD 20m USA b Department of Chemical and Biomolecular Engineering Case School of Engineering Case Westem Reserve University Cleveland, OH 44106, USA cspace science Institute, 4750 walnut Boulder, CO 80301, USA d Department of Astronomy and Space Science, Oung Hee University, 1732, Deoweong-daerq Gineung-gu, Yongin-sl Gyeonggi-do 17104 South Korea e Deparnnent of Atmospheric Sciences, Texas University TX, USA

A R T I C L I N F O E

Article nist00'.•
Received 24 January 2022
Revised 14 April 2022
Accepted 15 April 2022
Available online 21 April 2022

Keywords:
Elastic lignt scattering patterns
Optical trapping
Particle orientation and morphology
Aerosol detection

A B S T R A C T

We demonstrate a method for recording 2D forward-scattering patterns from optically trapped single airborne particles at multiple angular orientations. We collected images of trapped particles simultaneously with their scattering patterns to observe changes in the patterns with orientation. We present measurements of particles with wide-ranging morphologies from nearly spherical to highly irregular and with various compositions. The highly irregularly shaped particles have scattering patterns with spots of high intensity whose locations change with particle orientation. Additionally. measurements of a manufactured polystyrene spheroid of a known size are compared with calculated diffraction patterns, Such controlledorientation measurements have the potential to help develop algorithms to characterize airborne aerosol particles using morphological information inferred from remote-sensing or other elastic light scattering measurements.

I. Introduction

Elastic light-scattering patterns that are resolved in the polar (0) and azimuthal (4) angular dimensions contain valuable identiWing information about aerosol particles, such as size, shape, and wavelength-dependent refractive index [1,2]. Elastic light scattering is the result of incident photons that scatter from a material and remain unchanged in energy/wavelength, in contrast to the inelastic processes of fluorescence, phosphorescence emission, and Raman scattering. While spectroscopic methods of detection and characterization of aerosols, such as Raman spectroscopy, laserinduced breakdown spectrometry (LIBS), or cavity ring-down spectroscow can give detailed information about chemical and optical properties, elastic light scattering is particularly sensitive to particle size, shape, surface texture, and internal structure e.g,, [3-6]. Hence, elastic light scattering has the potential to be used in combination with other methods to classiß' the types of aerosols that populate a particular environment. The best way to develop tools to characterize particles based on elastic light scattering is to perform benchmarking experiments.

In the laboratory, these angularly dependent light-scattering patterns can be recorded from a single, isolated particle or a small ensemble of particles. Fitting these experimental scattering data to extract the physical properties of particles requires a robust light-scattering theow. One approach to link light-scattering experiments with theoretical computation is to trap single particles for detailed measurements. This can be accomplished with electrostatic trapping [7,81 or using optical trapping typically at visible wavelengths (see recent reviews by Gong et al. [9], Kalume et al. [101, Romanov and Yurkin [Il l).

* Corresponding author.
E-mail address: jessy.arnold@gmail.com (JA. Arnold).

https://doi.orgno.1016/j.jqsrt.2022.108223
0022-4073/0 2022 Elsevier Ltd. All rights reserved.

When particle dimensions are much smaller than the wavelength, they fall into the Rayleigh scattering regime, and their scattering can be determined using the electrostatic approximation [12]. For spherical, wavelength-scale particles, measurements can be compared to results computed with the Lorenz—Mie formulas [121. Thus far a number of uses for angular scattering patterns at visible wavelengths have been applied to particles that are close to spherical. These include sizing of individual liquid droplets [13,141 and polystyrene beads [15,161 as well as testing modified Lorenz—Mie models for core-shell droplet models [17]. Additionally, light-scattering intensity has been used to track changes in absorption properties of bacterial spores during germination [18].

Many microscopic aerosol particles of interest are both complex in shape and also significantly larger than the illuminating wavelengths. These particles produce complex light-scattering patterns that change with orientation relative to the direction of incident light. Even biological cells that have relatively simple, but non-spherical shapes show orientation-dependent light scattering [191. It has been shown that machine learning can be used to categorize particles according to morphology [20-221. However, these results were based on testing computed scattering patterns against a training data set that was also computationally generated. Controlled rotation of particles makes it possible to obtain multiple light-scattering patterns that can be used in such algorithms to make such classifications significantly more robust. Although in theow elastic scattering patterns as a function of 9 and contain a great deal of information about particle shape, the lack of experimental verification makes practical use of this information diffcult.

A number of works have reported experimental data of 2D angular light-scattering patterns for complex particles. These works have examined both the fonvard-scattering [23-251 and backscattering [24,26-28] regimes of non-spherical particles. Scattering patterns have been analyzed as a function of size and morphol0B' [4,5,19,27,28], but the capability to analyze the same particle at different, precisely known orientations presents an experimental challenge. Previous methods for gathering orientation-dependent data require multiple detectors or moving the detector during data collection [7,29–31]. In this paper, we combine optical trapping with a recently developed method [321 to control the angular orientation of the captured particle and present 2D elastic scattering patterns collected for the same particle in multiple orientations. In this experiment we also collect resolved microscope images of each particle studied for comparison with the scattering images, however a real-world aerosol identification system may not include microscope imaging. Moreover, as noted previously, the light scattering signal contains information about the internal structure as well as 3D shape and surface texture that can aid classification which cannot be gleaned from a resolved image.

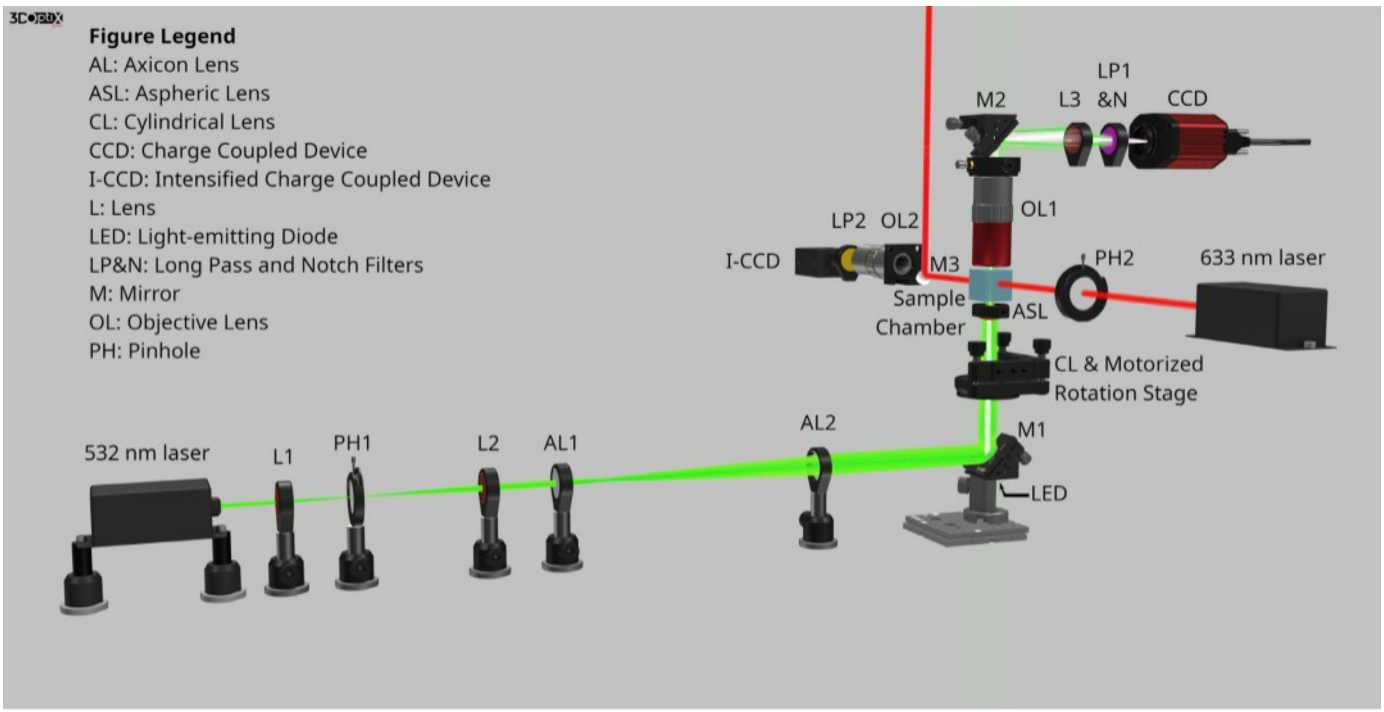

Fig. 1. 3D schematic or the experimental setup ror measuring elastic light scattering or an optically trapped single particle whose angular orientation can be controlled. A green (532 nm) trapping laser beam is positioned along one axis and a red (633 nm) laser beam is positioned along another axis 900 [rom the trapping beam. The red laser is used ror illumination or the particle to produce scattering patterns. Details or the rotation stage and beam geometry at the trapping region are described in the text. (For interpretation or the references to color in this figure legend, the reader is referred to the web version or this article.)

2. Setup for 2D oriented elastic scattering measurements

2.1. Optical trapping and angular orientation control

Fig. 1 shows a 3D illustration of our setup for optical trapping, angular orientation control, and 2D scattering-pattern recording from single airborne aerosol particles. The trapping mechanism is similar to that described by Redding and Pan [331 and consists of a circular, hollow laser beam brought to a focus by an aspheric lens into a hollow cone. In this configuration, the trapping forces resulting from the hollow conical beam have both an upward vertical component that balances the gravitational force and a horizontal component that strengthens the trap stability. The vertical component is the result of the radiation-pressure scattering force produced by the transfer of momentum from incident photons to the particle. The horizontal component results from the radiationpressure gradient force that tends to pull the particle in the direction of the field gradient, towards the focal point. For an absorbing particle, the trapping is also influenced by the photophoretic forces resulting from thermal processes whose magnitude and direction depend on the particle composition and morpholow.

A 532 nm diode-pumped solid-state laser (DPSS) continuouswave (CW) laser produces the trapping beam. The laser has a maximum output power of 2W and produces a Gaussian beam. The beam is cleaned, expanded, and re-collimated by a pinhole and a pair of lenses (Ll, fl — 25 mm; L2, fl = 50 mm) and then shaped into a collimated, circular, hollow beam using two axicon lenses (Al and A2, apex angle = 130^0). A 45^0 mirror then reflects the hollow beam upwards, perpendicular to the original direction of propagation. An aspheric lens (ASL fl 12 mm) brings the hollow beam to a focus inside of a small containment glass cell (25 mm x 25 mm x 15 mm). The sample chamber reduces air movements that can destabilize the trapping and has a small hole in the top for introducing samples.

Orientation control of the optically trapped particle is achieved via the mechanism described in our recent paper [32] and briefly summarized here. Above the mirror, prior to the aspheric focusing lens, we place a long-focal-length cylindrical lens (CLI, fl = 5000 mm) mounted on a motorized rotation stage (Thor Labs KIOCRI). Since cylindrical lenses focus light only along one axis, it deforms the circular beam into an oval ring. Once this oval hollow beam is focused into an oval cone, this generates a trapping region with horizontal forces that are stronger along the shorter axis. As the lens is rotated by the stage, the axes of the trapping region rotate as well, inducing a torque on the particle that results in rotational motion.

Images showing the position and orientation of the trapped particle are recorded by a charge coupled device (CCD) camera. Illumination is provided by a white light-emitting diode (LED) that shines through a center hole in the 45^0 mirror beneath the cylindrical lens. A microscope objective (OLI, N.A. = 0.55, WD = 13 mm, tube lens fl 200 mm) is situated above the chamber to collect the images of the LED-illuminated particle. A second 45^0 mirror reflects the image from the objective first through a long-pass filter, then a notch filter that blocks stray light from the 532 nm trapping beam, and finally to the CCD. The CCD images of the trapped particles have an equivalent size of 0.15 um per pixel, calibrated by trapped polystyrene beads of known sizes.

2.2. Recording of elastic light scattering patterns

To collect elastic scattering measurements, a red 633 nm laser beam is directed at the particle perpendicular to the trapping axis. The forward-scattered laser light is collimated by an objective lens (OL2, f = 55 mm) placed at focal-length distance from the trapped particle, using the Abbe Sine conditions, and then collected by an intensified CCD (I-CCD, Andor iStar) camera. The 1.5" diameter lens is able to collect roughly 20^0 in the 0-angle for = 0^0 to 360^0 . To prevent

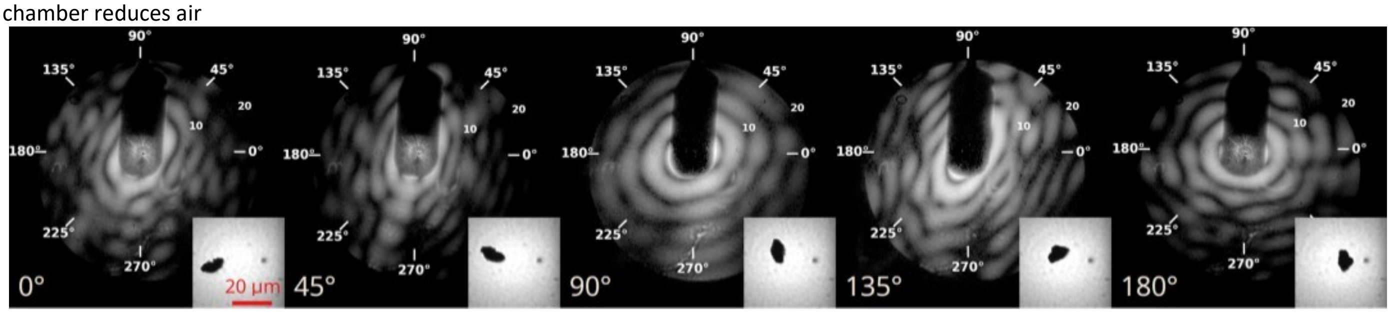

Fig. 2. Forward light-scattering patterns from a cluster or BG bacterial spores with a corresponding image inset at lower right or each panel. The position angle or the cylindrical lens is given in the Im•ver left or each panel. The scattering intensity is mapped to a log-scale.

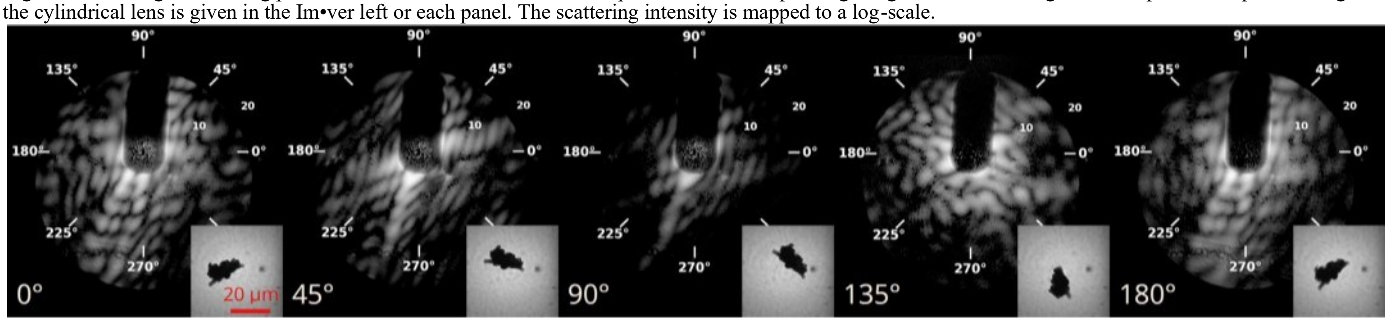

Fig. 3. Forward light-scattering patterns or a cluster or birch pollen grains with a corresponding image inset at 1m.ver right or each panel. The position angle or the cylindrical lens is given in the 10%'er left or each panel. The scattering intensity is mapped to a log-scale.

Fig.

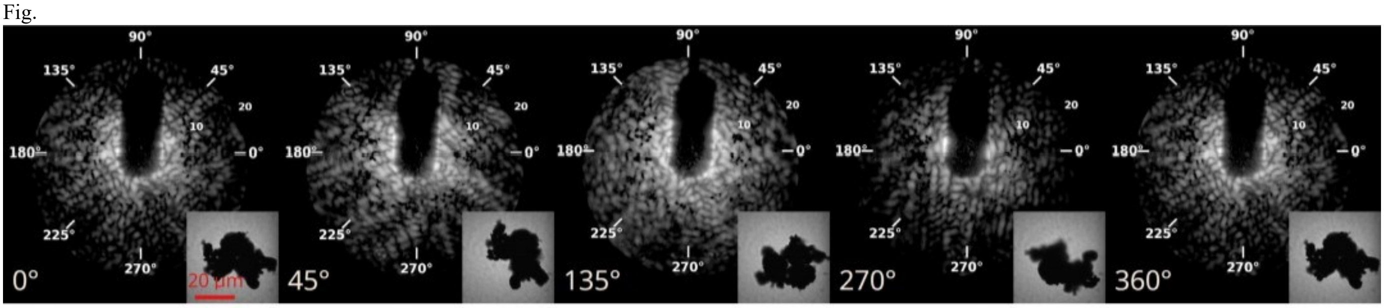

ﬁig. 4. Forward light-scattering patterns of a carbon nanotube cluster with a corresponding image inset at lower right of each panel. The position angle of the cylindrica

4. Forward light-scattering patterns or a carbon nanotube cluster with a corresponding image inset at lower right or each panel. The position angle the cylindrical lens is given in the 1m.ver left or each panel. The scattering intensity is mapped to a log-scale.

saturation of the I-CCD a 3 mm diameter, 45^0 small mirror (M3) blocks the very center of the forward-scattered beam, deflecting the intense 9 = 0^0 to 2.5^0 angle portion upward. A long-pass filter (LP2) is placed in front of the I-CCD to block any stray light from the 532 nm trapping beam. After each sequence of patterns from a given trapped particle is collected, the particle is released and a background pattern without the particle is collected to minimize background noise and stray reflections from the sample chamber in the data. During the collection of scattering patterns for a given particle at various orientations, the position and power of the 633 nm laser stays fixed so that the same background pattern can be used for all of the patterns in a series. It is not fea- Sible to collect a background frame for each pattern because that would necessitate interruption of trapping.

3. Recorded 2D elastic light-scattering patterns at different orientation

Using the apparatus described in Section 2, we collected forward-scattering patterns of an assortment of different aerosol particles with varying shapes and surface textures at different orientations. These are a cluster of Bacillus subtilis var. globigii (BG) bacterial spores, a cluster of Johnson grass pollen grains, a cluster of birch pollen grains,

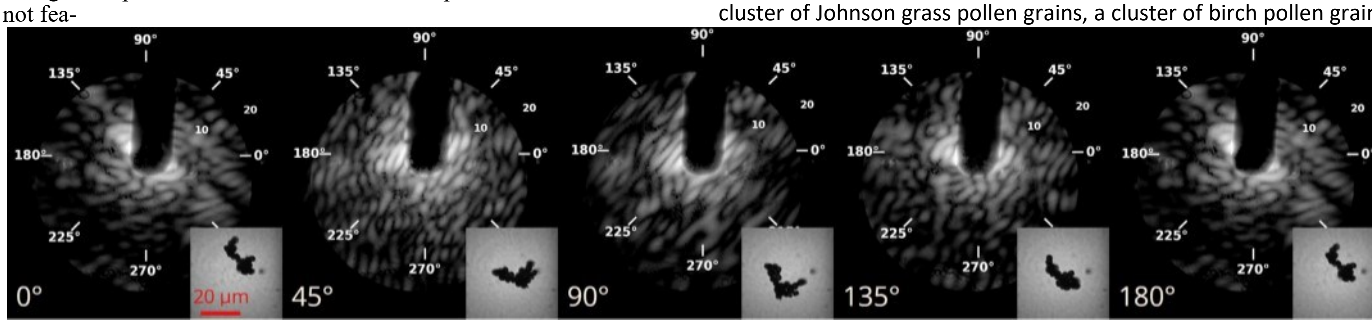

Fig. 5. Forward light-scattering patterns or a Johnson grass pollen cluster with a corresponding image inset at lower right or each panel. The position angle or the cylindrical lens is given in the Im•ver left or each panel. The scattering intensity is mapped to a log-scale.

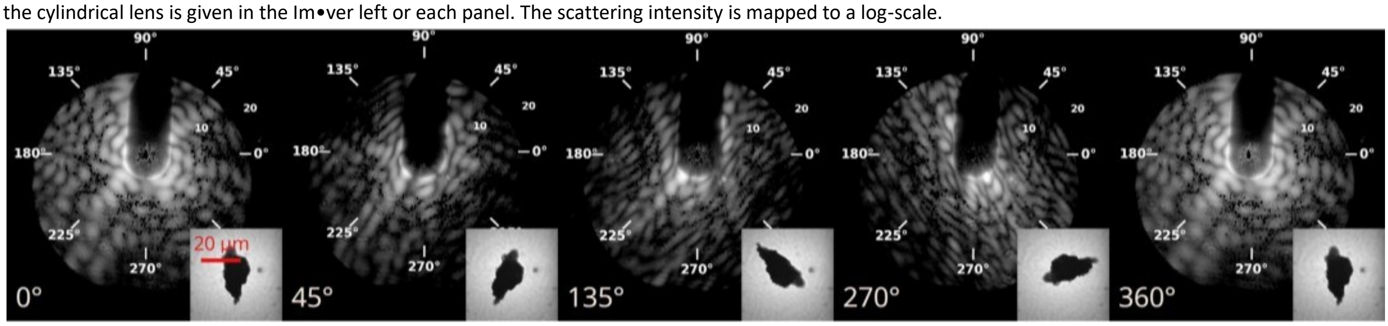

Fig. 6. Forward light-scattering patterns or a JSCM-I Mars surface analog (palagonite) grain with a corresponding image inset at lower right or each panel. The position angle or the cylindrical lens is given in the 10%'er left or each panel. The scattering intensity is mapped to a log-scale.

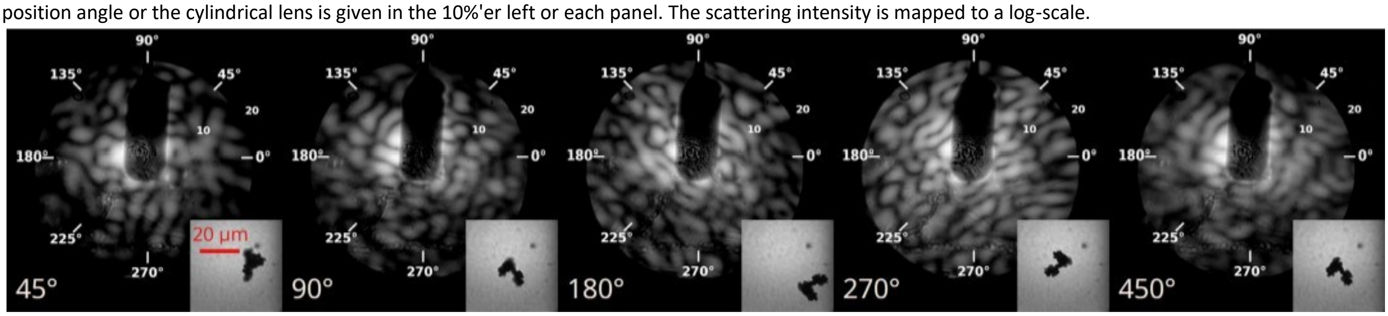

Fig. 7. Fotward light-scattering patterns ot a Tunisian dust aggregate with a corresponding image inset at 1m.ver right or each panel. The position angle or the cylindrical lens is given in the lower left or each panel. The scattering intensity is mapped to a log-scale.

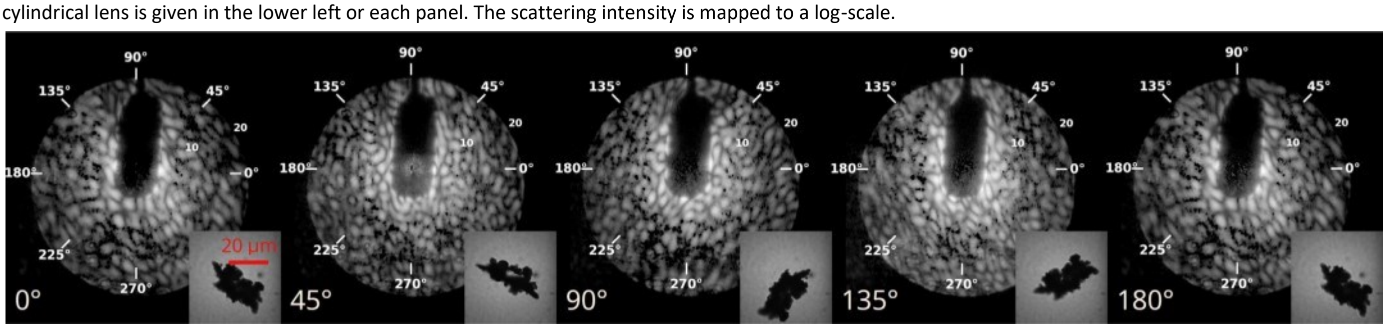

Fig. 8. Forward light-scattering patterns or a volcanic ash aggregate with a corresponding image inset at lower right of each panel. The position angle or the cylindrical lens is given in the lower left of each panel. The scattering intensity is mapped to a log-scale.

a cluster of carbon nano-tube, an aggregate of Tunisian dust, an aggregate of volcanic ash, a JSC-Mars (palagonite) grain, and a manufactured polystyrene spheroid. The sizes of the particles range from roughly 15 um to 80 pm. Each figure panel in Figs. 2-8 shows 2D fonvard-scattering pattern with the associated angular position of the cylindrical lens shown in the lower left. The intensity of each scattering pattern is mapped to a logarithmic scale. The inset in each panel at the lower right is the corresponding image of the particle at each measured orientation.

Cylindrical lens
position angle

450 3550

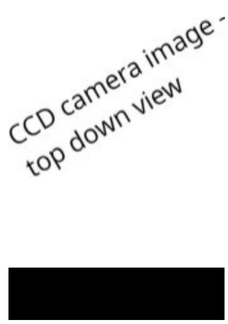
CCD camera image -
top down view

ana

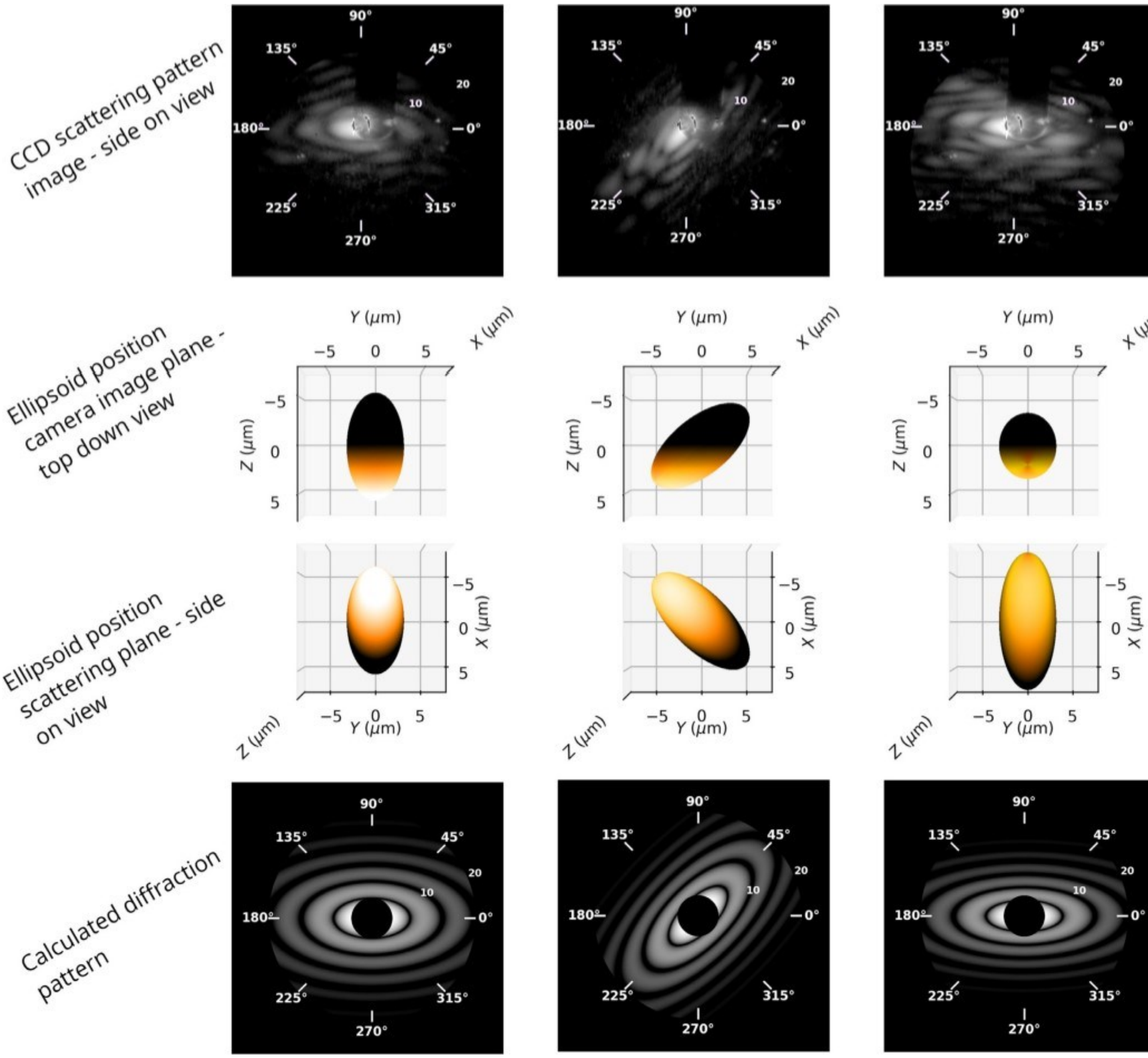

Fig. 9. Comparison of three different orientations of a spheroid of known size (CCD images in top row) with the resulting elastic light-scattering patterns (second row). The 3rd and 4th rows demonstrate the orientation or the spheroid in the imaging plane (c.f. the CCD images in the 1st rmv) and scattering laser incidence plane (cf. the scattering patterns in the 2nd respectively. The bottom rmv shows the calculated diffraction pattern or the spheroid in each orientation with a central mask the same angular size as the 45' mirror. The illumination and shading or the ellipsoids in the 3rd and 4th rows indicates the illumination direction of the scattering laser. The incident beam is oriented along the Z-axis and the Y-axis points um.vard. The azimuthal scattering angle is with respect to the X-axis.

The dark region near 90^0 extending from $9 = 0^0$ to 20^0 in the scattering patterns is the shadow of the small blocking mirror M3. In the inset image, the 633 nm laser illumination direction is from the bottom of the image towards the particle.

Figs. 2 -9 qualitatively demonstrate an inverse relationship between particle size and the angular scale of the islands in the scattering patterns. The particles less than 20 microns, that is, the BG cluster, Tunisian dust cluster, and polystyrene ellipsoid show a larger forward scattering lobe and larger scattering features with lower angular frequencies. BG spore clusters typically form a balllike shape with some surface texture due to the individual spores in the cluster. So, we would expect the forward-scattering pattern, which is dominated by diffraction, to appear as a series of concentric rings and not show a significant dependence on orientation. And indeed compared with the other particles of similar size such as the birch pollen grains or Johnson grass spore cluster, the BG spore cluster patterns do not change as much. However, this cluster is slightly elongated and therefore in some orientations the ring pattern is elongated and slightly broken, while in other orientations the ring pattern is closer to circular.

In contrast, for the other measured particles, there are obvious bright spots in the intensity patterns due to the highly irregular shapes of the particles. These patterns change orientation as the particle rotates, The birch pollen cluster pattern has a brighter linear feature between 225 and 270 degrees azimuth in all orientations except at the 180 degree orientation. when the narrower part of the particle was directly pointed at the scattering laser. The palagonite grain scattering pattern has multiple linear features. The larger, highly textured samples such as carbon nanotube and volcanic ash have complex scattering patterns with a large number of tightly spaced features. The complexity makes it difficult to understand the orientation-dependence of the patterns by eye, but we expect that machine-learning algorithms would be able to differentiate such patterns and correctly classiW the particles, as they have previously been able to differentiate clusters composed of spheres from those composed of pill-shaped particles 120,211.

For most of the particles, trapping lasted long enough to rotate the particle more than 360^0, and pattern collection could be repeated at some of the orientations. The scattering patterns collected at these repeated orientations match those collected during the first rotation cycle. As noted in our recent work on the particle rotation method 132], the particles sometimes undergo a rotational jump perpendicular to the trapping beam axis. In these cases, we can see the intensity pattern change as a result of this out-ofplane motion. Another interesting feature of the orientation control method is that the spin-rotational behavior depends on the trapping laser power as well as particle size and composition. In some cases, the particle undergoes a 2:1 rotation rate moving 360^0 for every 180^0 of revolution of the cylindrical lens; whereas, in other cases the rotation rate is 1:1.

4. Diffraction pattern calculations and comparisons with measured spheroid 2D scattering patterns

The well-defined geometry of manufactured polystyrene spheroids allows us to make comparisons with calculations. We produced spheroids with a well-established film stretching technique having a 2.5:1 aspect ratio that are 15 pm along the long axis and 6 um along the short axis [34,351. Due to the relatively large size of the spheroid compared with the wavelength of the 633 nm red laser, we compute the diffraction pattern as that dominates the small-angle forward scattering. As discussed in ref. [36], once the projected surface area of an ellipsoid is calculated, the amplitude scattering matrix reduces to a relatively simple expression. In our case, two of the ellipsoid axes are the same.

6

We use the spheroid images collected simultaneously with the forward-scattering patterns to ascertain the orientation of the spheroid with respect to the incident scattering beam (top row of Fig. 9). From the image we see that the ellipsoid has some slight asymmetries, possibly from accumulated dust in the sample chamber. The calculated patterns are shown in the bottom row of Fig. 9 with the measured patterns on the second row. We also show diagrams of how the ellipsoid is oriented with respect to the imaging plane (top-down view) and scattering plane (side-on view). The calculated diffraction patterns have a similar angular distribution of intensity; however, we can see some breaks in the expected oval rings in the measured pattern, probably due to the small irregularities in the particle.

5. Conclusion

We have demonstrated that a single optically trapped particle can be manipulated and that elastic scattering patterns can be collected for the same particle in multiple, known orientations. With this method there is no need to move the source or detector to record the orientation-dependant signal of a given particle. We were also able to simultaneously collect images of the particle at each orientation where scattering patterns are collected. Using this apparatus, we were able to directly link changes in the forward-scattering pattern with particle shape and orientation. We collected such measurements for a number of different types of aerosol particles, including a cluster of BG bacteria spores, of carbon nano-tubes, of grass and tree pollen grains, a mineral sample, and a manufactured polystyrene spheroid. Particles with complex morphology, such as the carbon nano-tube cluster, show a distinct speckle pattern that tracks with particle orientation. For particle systems that are close to spherical in shape, such as the cluster of BG spores, these orientation-dependent differences are less pronounced. Collecting images simultaneously with the scattering patterns allowed us to determine orientations of a manufacture spheroid for comparison to calculated diffraction patterns. Such capability provides additional information that can be used to classify particles using machine-learning or other techniques from elastic light scattering measurements.

Funding

This research was performed while the author held an NRC Research Associateship award at the Army Research Laboratory and funded through Defense Threat Reduction Agency (DTRA) (HDTRA1-17-D0002).

Declaration of Competing Interest

Authors declare that they have no conflict of interest.

References

Wriedt T. A review of elastic light scattering theories. Part Part Syst Charact

[21 Mishchenko MI, Travis LD, Lacis AA. Scattering, absorption, and emission of light by small particles. Cambridge University Press; 2002.

[31 Kerker M, Chew H, McNulty P, Kratohvil J, Cooke D, Sculley M, Lee M. Light scattering and fluorescence by small particles having internal structure. J Histocnem cytocnem1979;27(1

[41 Pan Y-L Aptowicz KB, Chang RK, Hart M, Eversole JD. Characterizing and monitoring respiratory aerosols by light scattering. Opt Lett 2003;28(8):589-91.

[51 Aptowicz K, Pinnick R, Hill S, Pan Y, Chang R. Optical scattering patterns from single urban aerosol particles at Adelphi, Maryland, USA: a classification relating to particle morphologies. J Geoplws Res 2006;111(D12). doi:10.1029/ 2005JD006774.

[61 Pan Y-L Berg M], Zhang SS-M, Noh H, Cao H, Chang RK, Videen G. Measurement and autocorrelation analysis or two-dimensional light-scattering patterns from living cells ror label-free classification. Cytom Part A 2011;79(4):284-92.

[71 Gucker n, Egan J]. Measurement or the angular variation or light scattered from single aerosol droplets. J Colloid Sci 1961 ; 16(1):68-84.

181 Barnes MD, Lermer N, Whitten WB, Ramsey JM. A CCD based approach to high-precision size and refractive index determination or levitated microdroplets using rraunhorer diffraction. Rev Sci Instrum 1997 ;68:2287-91.

191 Gong Z, Pan Y-L Videen G, Wang C. Optical trapping and manipulation or single particles in air: principles, technical details, and applications J Quant Spectrosc Radiat Transr 201 8 ;214:94–119、 2 1 4

1101 Kalume A, Wang C, Pan Y-L Optical-trapping laser techniques for characterizing airborne aerosol particles and its application in chemical aerosol study.

Micromachines 2021;12(4):466.

[11] Romanov AV, Yurkin MA. Single-particle characterization by elastic light scattering. Laser Photonics Rev 2021;15(2):2000368.

1221 Ding C. Convolutional neural networks ror particle shape classification using light-scattering patterns. J Quant Spectrosc Radiat Transr 2020;245: 106901.

1231 Ashkin A, Dziedzic J. Observation or light scattering from nonspherical particles using optical levitation. Appl Opt 1980; 19(5):660-8.

1241 Fernandes GE, Pan Chang RK, Aptowicz K, Pinnick RG. Simultaneous rorward-and backward-hemisphere elastic-light-scattering patterns or respirablesize aerosols. opt Lett 2006，31(20):3034–6.

1251 Ulanowski Hirst E, Kaye PH, Greenaway R. Retrieving the size of particles

Micromacnines 2021 ;

with rough and complex surfaces from two-dimensional scattering patterns. J Quant spectrosc Radiat Transr2012;113(18):2457–64.

1261 Heffernan BM, Heinson YVV, Maughan JB, Chakrabarti Sorensen CM.

1121 Bonren CF, Huffman DR. Absorption and scattering of light ty small particles. JOhn Wiley & sons; 2008.
1131 Guillon M, Dholakia K, McGloin D. Optical trapping and spectral analysis or aerosols with a supercontiuum laser source. Opt Express 2008: 11):7655-64.
1141 Carruthers AE, Reid JP, Orr-Ewing AJ. Longitudinal optical trapping and sizing or aerosol droplets. opt Express 2010;18(13): 14238-44. d0i:10.1364/OE.18. 014238.
1151 Doornbos RMP, schaerrer M, Hoekstra AG, S100t PMA. de C,rooth BG, Greve J. Elastic backscattering measurements or single biological cells in an optical trap. APPI opt 1996 . 3 5 (4):729–34.
1161 Jones SH, King MD, Ward AD. Determining the unique refractive index properties or solid polystyrene aerosol using broadband Mie scattering from optically trapped beads. Phys Chern Chem Phys 2013:15(47):20
1171 Kaiser T, Roll G, Schweiger G. Investigation or coated droplets in an optical trap: Raman-scattering, elastic-light-scattering, and evaporation characteristics. APPI opt 1996.,35(30):5918–24.
1181 Peng Chen D. Setlow P. Li Y-q. Elastic and inelastic light scattering from single bacterial spores in an optical trap allows the monitoring or spore germination dynamics. Anal Chem 2 009 . 8 1(10):4035–42.
1191 Watson D. Hagen N, Diver J, Marchand P, Chachisvilis M. Elastic light scattering from single cells: orientational dynamics in optical trap. Biophys J 2004;87(2):1298–306.
1201 Piedra P, Kalume A, Zubko E, Mackowski D, Pan Y-L, Videen G. Particle-shape classification using light scattering: an exercise in deep learning. J Quant Spectrosc Radiat Transr 2019231 : 140-56.
1211 Piedra P, Gobert C, Kalume A, Pan Y-L Kociraj M, Muinonen K, et al. Where is the machine looking? Locating discriminative light-scattering features by class-activation mapping. J Quant Spectrosc Radiat Transr 2020;247: 106936.
Backscattering measurements or micron-sized spherical particles. Appl Opt 2016;55(12):3214–18.
1271 Fu R, Wang C, Munoz O, Videen G, Santarpia J, Pan Y-L Elastic back-scattering patterns via particle surface roughness and orientation from single trapped airborne aerosol particles. J Quant Spectrosc Radiat Transr 2017;187:224-31. doi:10.1016/j.jqsrt.2016.09.018.
1281 Pan Y-L Wang C, Beresnev IA, Yutra AJ, Videen G, Ligon D, Santarpia JL Measurement or back-scattering patterns from single laser trapped aerosol particles in air. APPI opt 2017. 5 6(3) .. B 1
1291 Diehl S, Smith D. Sydor M. Analysis or suspended solids by single-particle scattering. APPI opt 1979:1 8 (1 0) . 1 6
1301 Wyatt P]. scnenrer KL, Phillips SD. Jackson C, Chang Y-J, parker RG, Phillips m, Bottiger JR. Aerosol particle analyzer. Appl Opt
1311 Kaye PH. Spatial light-scattering analysis as a means or characterizing and classirying non-spherical particles. Meas Sci Technol
1321 Arnold JA. Kalume A, Wang C, Videen G, Pan Y-L Active, controlled circular, and spin-rotational movement or optically trapped airborne micro-particles. opt 2021. 46(2 1) .. 5
1331 Redding B, Pan Y-L Optical trap ror both transparent and absorbing particles in air using a single shaped laser beam. Opt Lett 2015;40(12):2798–801. doi: 10. 1364/0L40002798.
1341 Ho C. Keller A, Odell J. Ottewill R. Preparation or monodisperse ellipsoidal polystyrene particles. C0110id potym sci
1351 Yan J, Rashidi A, Wirth CL Single and ensemble response or colloidal ellipsoids to a nearby ac electrode. colloids surr A 125384.
1361 Bi L, Yang P, Kattawar CNN, Kahn R. Single-scattering properties or triaxial ellipsoidal particles ror a size parameter range [rom the rayleign to geometric-optics regimes. Appl Opt 2 0 09 . 4 8(1):114–26.